ACS APPLIED MATERIALS & INTERFACES

Research Article

www.acsami.org

Preparation, Characterization, In Vitro Bioactivity, and Cellular Responses to a Polyetheretherketone Bioactive Composite Containing Nanocalcium Silicate for Bone Repair

Rui Ma,[†] Songchao Tang,[‡] Honglue Tan,[†] Jun Qian,[‡] Wentao Lin,[†] Yugang Wang,[†] Changsheng Liu,[‡] Jie Wei,*[,‡] and Tingting Tang*[,†]

[†]Shanghai Key Laboratory of Orthopedic Implants, Department of Orthopedic Surgery, Shanghai Ninth People's Hospital, Shanghai Jiao Tong University School of Medicine, Shanghai 200011, China

[‡]Key Laboratory for Ultrafine Materials of Ministry of Education, East China University of Science and Technology, Shanghai 200237, China

ABSTRACT: In this study, a nanocalcium silicate (n-CS)/polyetheretherketone (PEEK) bioactive composite was prepared using a process of compounding and injection-molding. The mechanical properties, hydrophilicity, and in vitro bioactivity of the composite, as well as the cellular responses of MC3T3-E1 cells (attachment, proliferation, spreading, and differentiation) to the composite, were investigated. The results showed that the mechanical properties and hydrophilicity of the composites were significantly improved by the addition of n-CS to PEEK. In addition, an apatite-layer formed on the composite surface after immersion in simulated body fluid (SBF) for 7 days. In cell culture tests, the results revealed that the n-CS/PEEK composite significantly promoted cell attachment, proliferation, and spreading compared with PEEK or ultrahigh molecular weight polyethylene (UHMWPE). Moreover, cells grown on the composite exhibited higher alkaline phosphatase (ALP) activity, more calcium nodule-formation, and higher expression levels of osteogenic differentiation-related genes than cells grown on PEEK or UHMWPE. These results indicated that the incorporation of n-CS to PEEK could greatly improve the bioactivity and biocompatibility of the composite. Thus, the n-CS/PEEK composite may be a promising bone repair material for use in orthopedic clinics.

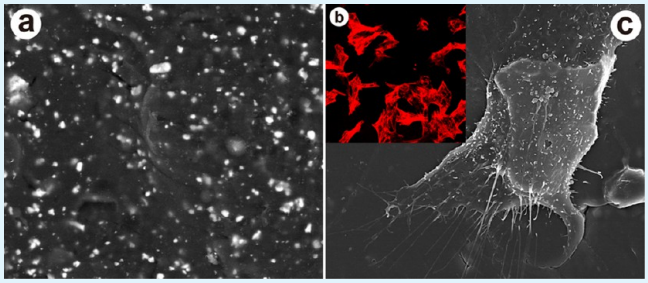

KEYWORDS: *polyetheretherketone, calcium silicate, composite, bioactivity, cellular responses*

1. INTRODUCTION

Bioactive materials, such as hydroxyapatite,[1−3] bioactive glass,[4] and glass-ceramics,[5,6] can enhance the proliferation and differentiation of osteoblasts in vitro and spontaneously bond to living bone without the formation of a surrounding fibrous tissue in vivo.[7,8] These bioactive inorganic materials with bone-bonding ability can efficiently osseointegrate with natural bone tissue.[9,10] Bioactive materials can create a bone-like apatite layer on their surface after implantation in vivo, and apatite formation is believed to be the main requirement for this bone-binding ability.[11]

Polyetheretherketone (PEEK), a semicrystalline and thermoplastic polymeric material, exhibits good biocompatibility, stable chemical resistance, and high thermal stability.[12] Furthermore, PEEK has been demonstrated to possess biomechanical properties (such as elastic modulus) that are similar to those of natural human bone, which could effectively reduce the stress shielding effect that is often observed in the application of conventional metallic implants.[13] Since receiving U.S. FDA approval in the late 1990s, PEEK has been extensively used as an implantable material for spinal, trauma, and orthopedic applications.[14] However, PEEK is a bioinert material, eliciting no positive response in the body.[15] After bioinert materials are implanted into a living body, an encapsulation of fibrous tissue forms and isolates the implants from the surrounding bone tissues.[16] Long-term clinical observations indicate that the primary causes of failure of bioinert implants involve nonstable implant fixation to the bone tissue.[17] Therefore, the major obstacle of PEEK is its bioinert nature, which reduces the efficiency of osseointegration at the bone/implant interface.

Recently, calcium silicate ($CaSiO_3$, CS) has been investigated as a bioactive material for bone repair.[18−20] CS has been reported to exhibit excellent in vitro bioactivity, and the formation of apatite on CS has been shown to be faster than the formation observed on bioglass or glass-ceramics in simulated body fluid (SBF).[21] Studies have demonstrated that CS is biocompatible and bioactive, with the ability to stimulate the proliferation and osteogenic differentiation of osteoblasts and bone-marrow mesenchymal stem cells.[22−24] Nevertheless, CS is brittle, as is other inorganic materials, and is only available in limited sites in the body.

Received: March 17, 2014
Accepted: July 11, 2014
Published: July 11, 2014

dx.doi.org/10.1021/am504409q | *ACS Appl. Mater. Interfaces* 2014, 6, 12214−12225

Many studies focused on composites created by combining polymers (flexibility) and inorganic materials (bioactivity).[25−28] Therefore, in the present study, a bioactive composite was prepared by incorporating n-CS into a PEEK matrix using a compounding and injection-molding technique, and the mechanical properties, hydrophilicity, and in vitro bioactivity, as well as the cellular responses to the composite, were evaluated.

2. MATERIALS AND METHODS

2.1. Preparation of n-CS. n-CS was synthesized from $Ca(NO_3)_2 \cdot 4H_2O$ and $Na_2SiO_3 \cdot 9H_2O$ ($Ca(NO_3)_2 \cdot 4H_2O/Na_2SiO_3 \cdot 9H_2O$ (molar ratio) = 1:1) using a chemical precipitation method. The two reagents were dissolved in deionized water in separate beakers. The concentrations were adjusted to 0.5 M, and 0.2% polyethylene glycol was added into 300 mL of $Ca(NO_3)_2$ solution at ambient temperature. Under stirring, 300 mL of the Na_2SiO_3 solution was added dropwise into the $Ca(NO_3)_2$ solution to generate a $CaSiO_3$ precipitate. Then, 300 mL of dimethylformamide (DMF) was added to the beakers, and the mixture was hydrothermally treated under magnetic stirring. The temperature was gradually increased to 120 °C and held for 5 h to evaporate the water; then, the DMF was extracted. The precipitate was thoroughly washed with deionized water and then dried in an oven at 60 °C to produce powdered n-CS samples.

2.2. Preparation of the n-CS/PEEK Composites. PEEK powder with a mean particle size of 20 μm was obtained from Victrex Manufacturing Ltd. (South Yorkshire, U.K.). The n-CS/PEEK composites with 20, 40, and 60 wt % n-CS content were prepared via a compounding and injection-molding process. The n-CS powder and PEEK powder were compounded in a high-speed ball mill (QM-3B, Nanjing T-Bota Scietech Instruments & Equipment Ltd., Nanjing, China) at a mixing speed of 500 rpm for 1 h, and the mixtures were dried at 150 °C for 24 h. The n-CS/PEEK composites were produced at an injection temperature of 380 °C from a mixture of n-CS and PEEK powders using an injection-molding machine (BA-300/050CD, Battenfeld, Awans, Belgium). The PEEK sample used as a control was prepared using the same method.

The n-CS/PEEK composite and PEEK samples were cut into discs with thicknesses of 2 mm and diameters of 15 mm or 34 mm using a turning lathe (C616-1, Jinan First Machine Tool Group Co. Ltd., Jinan, China). Then, all the samples were cleaned with deionized water for 2 h in an ultrasonic oscillator (B3500S-MT, Branson, Danbury, Connecticut, U.S.A.). After drying at 37 °C overnight, the samples were sterilized with ethylene oxide for 3 h. Finally, the sterilized samples were sealed in sterile containers for subsequent use.

2.3. Characterization of the n-CS/PEEK Composites. The surface morphology and chemical composition of the n-CS/PEEK composites and PEEK were characterized using scanning electron microscopy (SEM; S-4800, Hitachi, Tokyo, Japan) in backscattered electron mode, energy dispersive spectrometry (EDS; X-Max, Horiba, Kyoto, Japan), X-ray diffraction (XRD; Geigerflex, Rigaku Co., Akishima, Japan), and Fourier transform infrared spectroscopy (FTIR; S2000, PerkinElmer, Waltham, Massachusetts, U.S.A.).

The mechanical properties (including the elastic modulus, tensile strength, and compressive strength) of the samples were measured using a material testing machine (Instron 5567, Norwood, Massachusetts, U.S.A.) at a crosshead speed of 0.1 mm/min according to ASTM D790. The average of five readings for each sample was recorded.

The hydrophilic properties of the surfaces of the n-CS/PEEK composites and PEEK were determined by measuring the static water contact angles using the sessile drop method on a drop-shape analysis system (JC-2000D3, Shanghai Zhongcheng Digital Technology Co., Shanghai, China) at ambient temperature and humidity. Five measurements were performed at different points of each sample.

By evaluating the mechanical and hydrophilic properties of the n-CS/PEEK composites with different n-CS contents, a composite with an optimal n-CS content (40 wt %) was selected to perform the following studies.

2.4. Apatite-Formation on the Composite. The in vitro bioactivity of an artificial material can be evaluated by examining the formation of apatite on its surface in SBF.[29] Samples of the n-CS/PEEK composite and PEEK with diameters of 15 mm were immersed in 40 mL of SBF at 37 °C in a humidified atmosphere for 7, 14, 21, and 28 days. At the end of each time point, the samples were rinsed three times with deionized water, dried overnight, sputter-coated with gold, and analyzed by SEM and EDS; additionally, the concentrations of calcium (Ca), phosphorus (P), and silicon (Si) ions in the soaked SBF were measured by inductively coupled plasma atomic emission spectroscopy (ICP-AES; Varian, Palo Alto, CA, U.S.A.).

Table 1. Primers for Real-Time PCR

target genes	primer sequences (5′−3′)
ALP	F: GGGCATTGTGACTACCACTCG
	R: CCTCTGGTGGCATCTCGTTAT
COL 1	F: AACAGTCGCTTCACCTACAGC
	R: GGTCTTGGTGGTTTTGTATTCG
OPN	F: CTTTCACTCCAATCGTCCCTAC
	R: CCTTAGACTCACCGCTCTTCAT
OC	F: GGACCATCTTTCTGCTCACTCTG
	R: TTCACTACCTTATTGCCCTCCTG
β-actin	F: GAGACCTTCAACACCCCAGC
	R: ATGTCACGCACGATTTCCC

2.5. Cell Culture. To investigate the interaction between cells and the n-CS/PEEK composite (with PEEK used as a control), MC3T3-E1 cells (a mouse preosteoblastic cell line derived from mouse calvaria) were used in this study. The cells were cultured in Dulbecco's Modified Eagle Medium (DMEM; Hyclone, Thermo Fisher Scientific Inc., Miami, FL, U.S.A.) supplemented with 10% fetal bovine serum (FBS; GibcoBRL, Grand Island, NY, U.S.A.), 1% penicillin (100 U/mL; GibcoBRL), and streptomycin sulfate (100 mg/mL; GibcoBRL) at 37 °C in a humidified atmosphere with 5% CO_2 and 95% air. The culture medium was changed every 3 days. An ultrahigh molecular weight polyethylene (UHMWPE) slab with a molecular weight of two million was obtained from Roechling Engineering Plastics Ltd. (Munich, Germany) and was used as another control for the cell tests. The preparation method of UHMWPE samples was similar to that of the n-CS/PEEK composites and PEEK.

2.5.1. Cell Attachment. A cell counting kit-8 (CCK-8) assay was used to analyze cell attachment at 6, 12, and 24 h. In advance, samples of the n-CS/PEEK composite with a diameter of 15 mm were placed into the wells of a 24-well plate (Costar, Corning Incorporated, NY, U.S.A.). Cultured MC3T3-E1 cells were digested with 0.25% trypsin (Sigma-Aldrich, St. Louis, Missouri, U.S.A.), resuspended with culture medium, counted using a cell viability analyzer (Vi-cell XR, Beckman Coulter Inc., Brea, CA, U.S.A.), and seeded in each well at a density of $3 \times 10^4/cm^2$, with empty wells containing DMEM as a blank control. The culture plates were incubated at 37 °C in a humidified atmosphere of 5% CO_2. At each time point, the samples were gently rinsed three times with phosphate-buffered saline (PBS; pH = 7.4) to remove the unattached cells and transferred to a new 24-well plate. A total of 50 μL of CCK-8 solution (Dojindo Molecular Technologies Inc., Kumamoto, Japan) was added to each well and incubated for 3 h. After this incubation, 100 μL of the supernatant was transferred into a 96-well plate and read at 450 nm using a microplate reader (Synergy HT, Biotek, Winooski, VT, U.S.A.) with 620 nm as the reference wavelength. The mean absorbance value/optical density (OD) obtained from the blank control was subtracted from the ODs of the test groups.

2.5.2. Cell Proliferation. Cell proliferation was also investigated using the CCK-8 assay. The cell seeding density was 1×10^4 /cm^2, and the detection time points were 1, 3, and 7 days. The other detailed procedures were nearly identical to those of the cell attachment test. The modified OD values at days 3 and 7 were normalized to those at day 1 because the numbers of attached cells grown on different samples were different at day 1.

2.5.3. Cell Morphology and Spreading. The cell morphology and spreading on the samples were observed via confocal laser scanning microscopy (CLSM) and SEM. During preparation of the cell samples for CLSM, the cell seeding procedures were similar to those of the cell attachment test. After culturing on the samples for 12 and 24 h, the cells

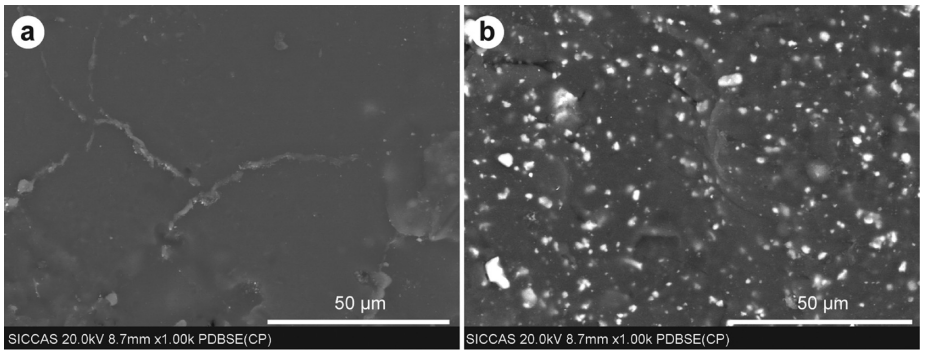

Figure 1. SEM images of PEEK (a) and the n-CS/PEEK composite (b) in backscattered electron mode. The white dots indicate CS.

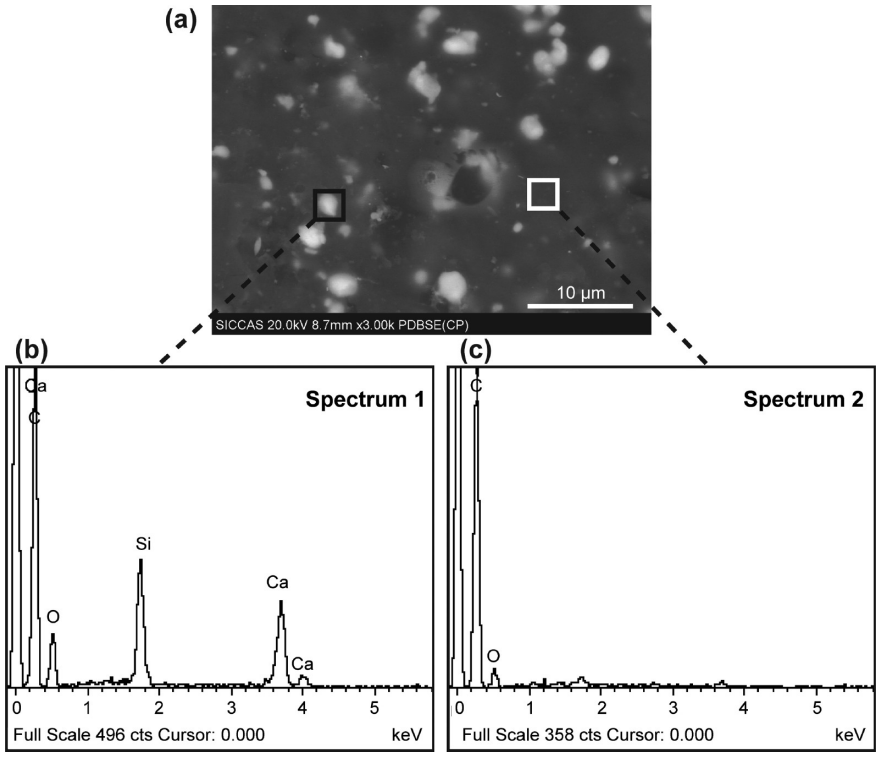

Figure 2. SEM image (a) and EDS spectra of the n-CS/PEEK composite surface: CS (b) and PEEK (c).

were gently washed three times with PBS, fixed with 4% paraformaldehyde for 15 min at room temperature, and permeabilized with 0.1% Triton X-100 in PBS for 10 min. The cells were stained with rhodamine-phalloidin (5 U/mL, Biotium, Hayward, CA, U.S.A.) for 30 min and washed three times with PBS (5 min for each washing). The filamentous actins of the cell cytoskeleton were visualized using a CLSM (TCS SP2, Leica, Heidelberg, Germany). To prepare the cell samples for SEM, MC3T3-E1 cells were seeded following the same procedures as in the cell proliferation test and cultured on the samples for 1, 3, and 7 days. At the end of each time point, the cells were fixed with 2.5% glutaraldehyde for 15 min and washed three times with PBS. Next, the cells were dehydrated with gradient ethanol at volume fractions of 30%, 50%, 70%, 90%, and 100% (10 min for each gradient). Subsequently, the ethanol was replaced by hexamethyldisilazane (HMDS, Sigma-Aldrich) for 10 min. Finally, all the samples were air-dried, sputter-coated with gold, and observed with SEM.

2.6. Cell Osteogenic Inductive Culture. MC3T3-E1 cells were seeded on the samples (similar to the above cell culture procedures) with a diameter of 34 mm at a density of $3 \times 10^4/cm^2$ in a 6-well plate containing samples. After 24 h, the culture medium was changed to the osteogenic inductive culture medium containing DMEM supplemented with 10% FBS, 1% penicillin (100 U/mL) and streptomycin sulfate (100 mg/mL), 100 nM dexamethasone (Sigma-Aldrich), 50 μg/mL ascorbic acid (Sigma-Aldrich), and 10 mM β-glycerophosphate sodium (Sigma-Aldrich). The osteogenic induction medium was replaced every other day.

2.6.1. Alkaline Phosphatase (ALP) Staining and ALP Activity Assay. After 7, 10, and 14 days of culture with the osteogenic inductive culture medium, ALP staining was carried out according to the procedure used in our previous study.[30] The ALP activity was determined by quantifying the amount of p-nitrophenol, the end product of hydrolyzed para-nitrophenyl phosphate using a microplate test kit (Nanjing Jiancheng Bioengineering Institute, Nanjing, China). The ODs were measured at 405 nm using a microplate reader (Synergy HT, Bio-Tek). Furthermore, the total protein content was determined using the BCA protein assay kit (Pierce, Thermo, Rockford, IL, U.S.A.) according to the manufacturer's protocol. Finally, the ALP activity was normalized to the corresponding content of total protein.

2.6.2. Alizarin Red Staining and Quantitative Analysis. Alizarin red staining was used to analyze calcium nodule formation (mineralization). Cells were grown on the samples for 21 and 28 days in osteogenic inductive culture medium, as described previously. The cells on the samples were then fixed in 4% paraformaldehyde for 15 min and stained with 1% alizarin red solution (pH = 4.20; Sigma-Aldrich) for 45 min at

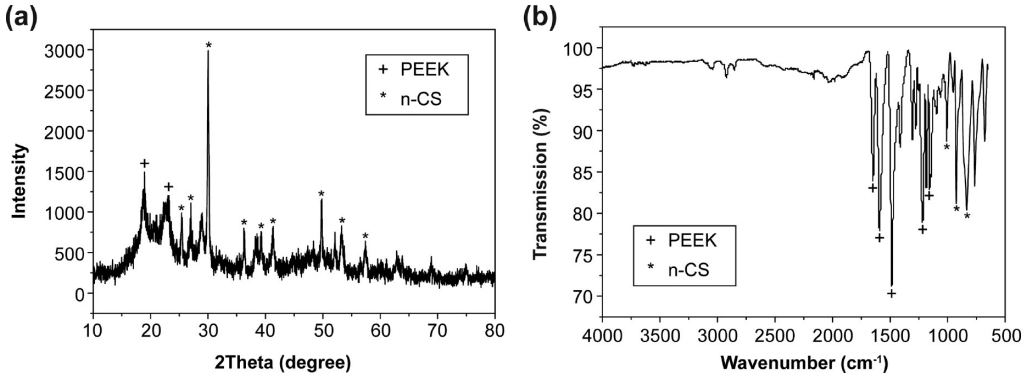

Figure 3. XRD (a) and FTIR (b) of the n-CS/PEEK composite; + represents PEEK and * indicates n-CS.

room temperature. Next, the samples were washed with deionized water until no further orange color appeared in the deionized water and then dried at 37 °C. Additionally, samples with no cells were stained with alizarin red solution as a blank control. Finally, images of all the stained samples were acquired using a digital scanner (Scanjet 2400, HP, Palo Alto, CA, U.S.A.). For quantitative analysis, the orange staining was dissolved in 10% cetylpyridinum chloride (pH = 7.0; Sigma-Aldrich) in 10 mM sodium phosphate (Sigma-Aldrich), and the ODs were measured at 620 nm using a microplate reader (Synergy HT, Bio-Tek). The mean ODs obtained from the blank control were subtracted from the ODs of the test groups.

2.6.3. Expression of Osteogenic Differentiation-Related Genes. The mRNA expression of osteogenic differentiation-related genes, that is, mouse alkaline phosphatase (ALP), collagen type I (COL 1), osteoprotein (OPN), and osteocalcin (OC), were quantitatively determined via real-time polymerase chain reaction (PCR). The transcription levels of the genes were normalized to that of the β-actin housekeeping gene. The sequences of the forward and reverse primers are shown in Table 1. Total RNA was collected from cells grown on the samples using the TRIzol reagent (Ambion, Grand Island, NY, U.S.A.) according to the manufacturer's protocol. Reverse transcription was performed following the protocol of the Revert-Aid first-strand cDNA synthesis kit (Fermentas, Thermo Scientific Molecular Biology, Pittsburgh, PA, U.S.A.). Quantitative real-time PCR was performed using the SYBR premix EX Taq PCR kit (TaKaRa Biotechnology Co., Dalian, China).

2.7. Statistical Analysis. All the data are presented as the means ± standard deviations, and all the experiments were repeated three times. The statistical significances between different groups were analyzed using a two-way analysis of variance (ANOVA) test, and multiple comparisons were performed using the least significant difference (LSD) test. A p-value < 0.05 was defined as significant, and a p-value < 0.01 was defined as highly significant.

3. RESULTS

3.1. SEM and EDS Analyses of the Composite. Figure 1 presents SEM images of PEEK and the 40 wt % n-CS/PEEK composite. Abundant CS particles with high electron density (white dots) were uniformly distributed on the composite surface, whereas no other composition existed on the PEEK surface. The EDS spectra of the composite is shown in Figure 2. Elemental peaks of Ca and Si were observed on the composite due to the CS particles, whereas no Ca or Si peaks appeared for the PEEK matrix.

3.2. XRD and FTIR Analyses of the Composite. Figure 3a presents the XRD pattern of the 40 wt % n-CS/PEEK composite. The diffraction peaks of the composite at approximately 2θ = 25.5°, 27°, 29.5°, 36°, 38.5°, 41°, 49.5°, 53°, and 57° are attributed to the characteristic peaks of n-CS, and the two peaks at approximately 2θ = 19° and 22.5° belong to the characteristic peaks of PEEK.[31,32] The results indicated that the composite contained both n-CS and PEEK.

Table 2. Mechanical Properties of the n-CS/PEEK Composites with Different n-CS Contents

samples	elastic modulus (GPa)	tensile strength (MPa)	compressive strength (MPa)
PEEK	2.3 ± 0.2	86 ± 1.5	108 ± 1.9
20 wt % n-CS/PEEK composite	3.2 ± 0.2	83 ± 2.1	126 ± 2.4
40 wt % n-CS/PEEK composite	4.4 ± 0.3	74 ± 2.2	152 ± 3.1
60 wt % n-CS/PEEK composite	3.8 ± 0.1	55 ± 2.0	90 ± 3.6

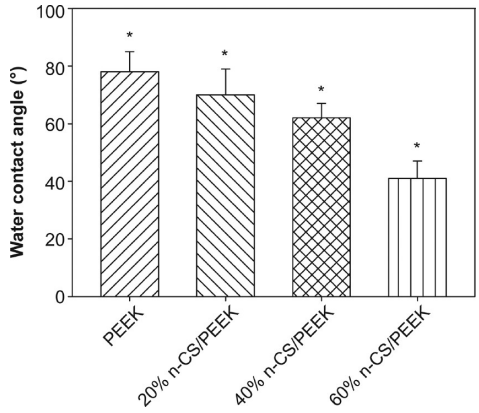

Figure 4. Quantitative measurement of water contact angles on PEEK and the n-CS/PEEK composites. "*" denotes significant differences compared with the other three groups (p < 0.05).

Figure 3b shows the FTIR pattern of the 40 wt % n-CS/PEEK composite. The peaks at 1650 and 1490 cm^{-1} are ascribed to diphenylketone; the peaks at 1188 and 1158 cm^{-1} are ascribed to C—O—C stretching vibration of the diaryl groups; and the peaks at 1600 cm^{-1} are related to the C═C bond in the benzene ring of PEEK.[32] The existence of Si—O was confirmed by the peaks at 950 and 810 cm^{-1}, and the peak at 1090 cm^{-1} belonged to the Si—O—Si bond.[31,33] The results also indicated that the composite contained both n-CS and PEEK.

3.3. Mechanical and Hydrophilic Properties of the Composites. Table 2 lists the mechanical properties of the n-CS/PEEK composites with different n-CS contents. The elastic modulus and compressive strength of the composites increased with the increase of the n-CS content from 0 to 40 wt %. Moreover, the tensile strength of the composites decreased slightly with increasing n-CS content and was lower than that of PEEK. The composite with 40 wt % n-CS resulted in the highest elastic

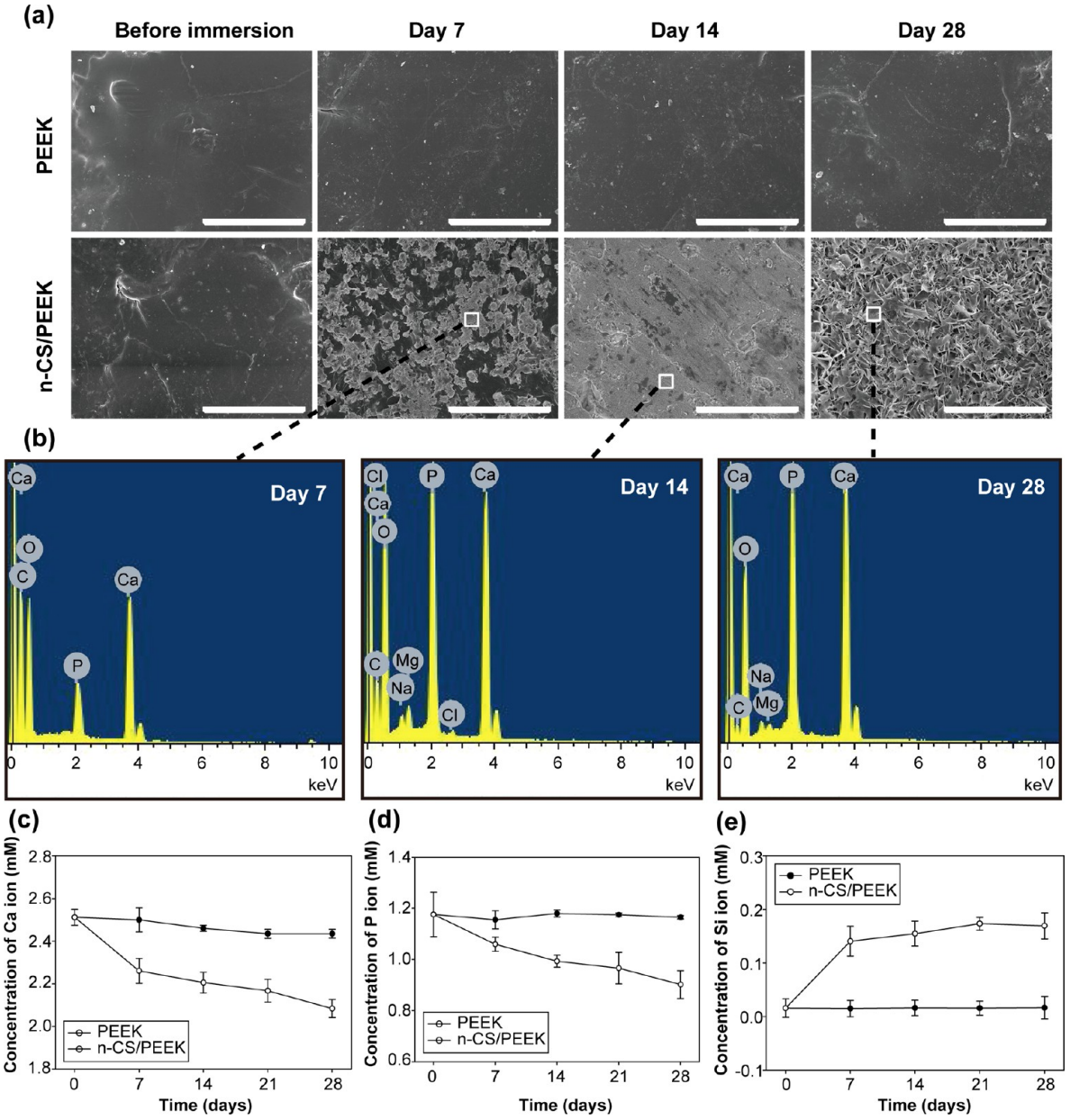

Figure 5. Apatite-formation on the n-CS/PEEK composite and PEEK after immersion in SBF: (a) SEM images showing the surface morphology of the n-CS/PEEK composite and PEEK before and after immersion in SBF for 7, 14, and 28 days (scale bar = 50 μm); (b) EDS spectra of the composite after immersion in SBF for 7, 14, and 28 days; (c–e) changes of ionic concentrations of Ca (c), P (d), and Si (e) ions in SBF after immersion for 7, 14, 21, and 28 days.

modulus of 4.4 GPa and highest compressive strength of 152 MPa, indicating that the incorporation of 40 wt % n-CS into PEEK enhanced the mechanical properties of the composite. However, the highest n-CS content of 60 wt % yielded a lower elastic modulus (3.8 GPa), tensile strength (55 MPa), and compressive strength (90 MPa) than the composite with 40 wt % n-CS content.

Figure 4 shows the results of the measurement of water contact angles. The water contact angles of PEEK and the n-CS/PEEK composites with 20, 40, and 60 wt % n-CS contents were 78 ± 7°, 70 ± 9°, 62 ± 5°, and 41 ± 6°, respectively. The water contact angles of the composites were significantly lower than that of PEEK ($p < 0.05$). These results indicated that the hydrophilicity of the n-CS/PEEK composites was improved by the addition of n-CS into PEEK compared with PEEK, which was n-CS content dependent.

3.4. Apatite Formation on the Composite in SBF. Figure 5a shows SEM images of the surface morphology of the n-CS/PEEK composite and PEEK before and after immersion in SBF for 7, 14, and 28 days. Many clustered apatite islands formed on the n-CS/PEEK composite surface after being soaked in SBF for 7 days. After 14 days, a newly formed apatite layer was observed on the n-CS/PEEK composite. After 28 days, a thick layer of apatite covered the entire surface of the composite, which was tile-shaped and compact. However, there was no newly formed substance on PEEK even after 28 days of immersion. Figure 5b shows the EDS spectra of the newly formed apatite on the composite. Ca and P peaks appeared on the surfaces of the composite at days 7, 14, and 28. Figure 5c–e shows the changes in the ionic concentrations in SBF after incubating with the composite after various time periods. The concentration of Ca ions decreased

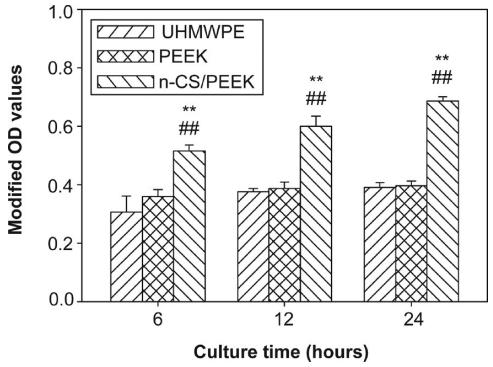

Figure 6. Cell attachment on UHMWPE, PEEK, and the n-CS/PEEK composite after 6, 12, and 24 h of culture. The modified ODs are ODs at 450 nm subtracted from OD_s at 620 nm and ODs of the blank control. "##" and "**" denote significant differences compared with UHMWPE and PEEK, respectively ($p < 0.01$).

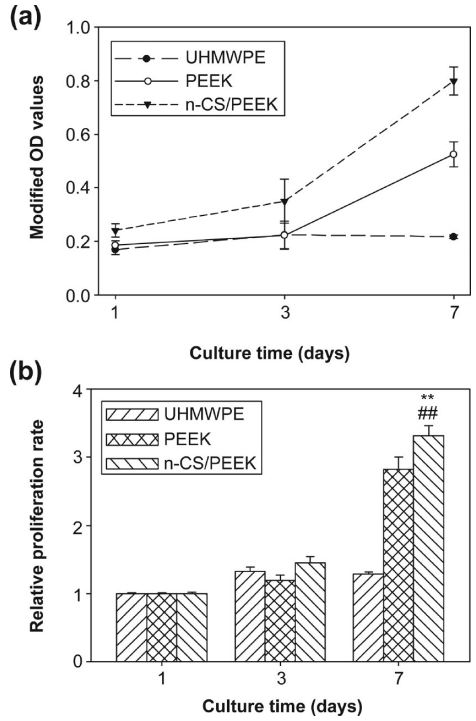

Figure 7. Cell proliferation on UHMWPE, PEEK, and the n-CS/PEEK composite after 1, 3, and 7 days of culture: (a) proliferative tendency of MC3T3-E1 cells; (b) relative proliferation rate of MC3T3-E1 cells. The modified ODs are ODs at 450 nm subtracted from ODs at 620 nm and ODs of the blank control. The modified ODs at day 3 and day 7 were normalized to those at day 1. "##" and "**" denote significant differences compared with UHMWPE and PEEK, respectively ($p < 0.01$).

drastically from day 1 to day 7 and subsequently reached a stably decreasing stage from day 7 to day 28 (Figure 5c). The P ions in SBF decreased gradually from day 0 to day 28 as shown in Figure 5d. A large amount of Si ions were released from the composite into the SBF from day 0 to day 7, fewer Si ions were released from day 7 to day 21, and no additional Si ions were released from day 21 to day 28 (Figure 5e). In contrast, no significant changes were observed for the concentrations of Ca, P, and Si ions in SBF after incubating with PEEK for various time periods.

3.5. Cell Attachment. Figure 6 presents the quantitative analysis of cell attachment on the material surfaces. After 6, 12, and 24 h of culture, more MC3T3-E1 cells were observed to attach on the n-CS/PEEK composite than on PEEK or UHMWPE ($p < 0.01$), indicating that the n-CS/PEEK composite could promote the attachment of MC3T3-E1 cells.

3.6. Cell Proliferation. The proliferation of MC3T3-E1 cells cultured on the material surfaces was analyzed using a CCK-8 assay as shown in Figure 7. Cells grown on the composite displayed a persistent increasing proliferation tendency from day 1 to day 7 ($p < 0.05$); however, cells grown on PEEK exhibited no significantly proliferative trend from day 1 to day 3; in addition, cells grown on UHMWPE exhibited no significantly proliferative trend from day 3 to day 7 ($p > 0.05$; Figure 7a). Furthermore, the relative proliferation rate of cells grown on the composite was significantly higher than those grown on PEEK or UHMWPE at day 7 ($p < 0.01$; Figure 7b).

3.7. Cell Morphology and Spreading. Figure 8 presents CLSM images of the cytoskeleton of phalloidin-stained MC3T3-E1 cells on the material surfaces. Cells grown on the composite were polygonal and clustered, whereas cells grown on PEEK or UHMWPE were dispersive. More actin filaments linking adjacent cells were observed at both 12 and 24 h in cells grown on the composite than on PEEK or UHMWPE.

SEM images showing the morphology of MC3T3-E1 cells grown on the materials are presented in Figure 9. After 1 day of culture, cells grown on the composite exhibited a flat morphology with many fine filopodia anchored at the composite surface, whereas cells grown on PEEK or UHMWPE were rod-like with few filopodia. A greater number of cells were observed on the composite with higher spreading efficiency at day 3, compared with cells grown on PEEK or UHMWPE. After 7 days of culture, cells grown on the composite and cells grown on PEEK proliferated to cover nearly the entire surface, while cells grown on UHMWPE exhibited no apparent proliferative trend from day 3 to day 7.

3.8. ALP Staining and ALP Activity Assay. Figure 10 shows the ALP staining and ALP activity of MC3T3-E1 cells grown on the material surfaces. The ALP staining on the n-CS/PEEK composite was considerably stronger than that on PEEK or UHMWPE at each time point (Figure 10a). Figure 10b shows the quantitative analysis of the ALP activity. The ALP activity on the n-CS/PEEK composite was significantly higher than that on PEEK or UHMWPE, which is consistent with the qualitative ALP staining results.

3.9. Alizarin Red Staining and Quantitative Analysis. Figure 11 presents the results of the alizarin red staining and its quantitative analysis on the material surfaces. More calcium nodules were formed on the n-CS/PEEK composite than on PEEK or UHMWPE (Figure 11a). Quantitative analysis of the alizarin red staining indicated that the composite exhibited clearly higher mineralization than PEEK or UHMWPE ($p < 0.01$; Figure 11b).

3.10. Expression of Osteogenic Differentiation-Related Genes. Figure 12 presents the results of real-time PCR of the osteogenic differentiation-related genes. At day 7, cells grown on the n-CS/PEEK composite showed obviously higher expression levels of ALP and COL 1 compared with those grown on PEEK or UHMWPE. At day 14, the ALP, COL 1, OPN, and OC mRNA levels of cells grown on the composite were significantly higher than those grown on PEEK or UHMWPE. At day 21, cells grown on the composite showed obviously higher expression levels of COL 1 and OC than cells grown on PEEK and obviously higher expression levels of COL1, OPN, and OC than cells grown on UHMWPE.

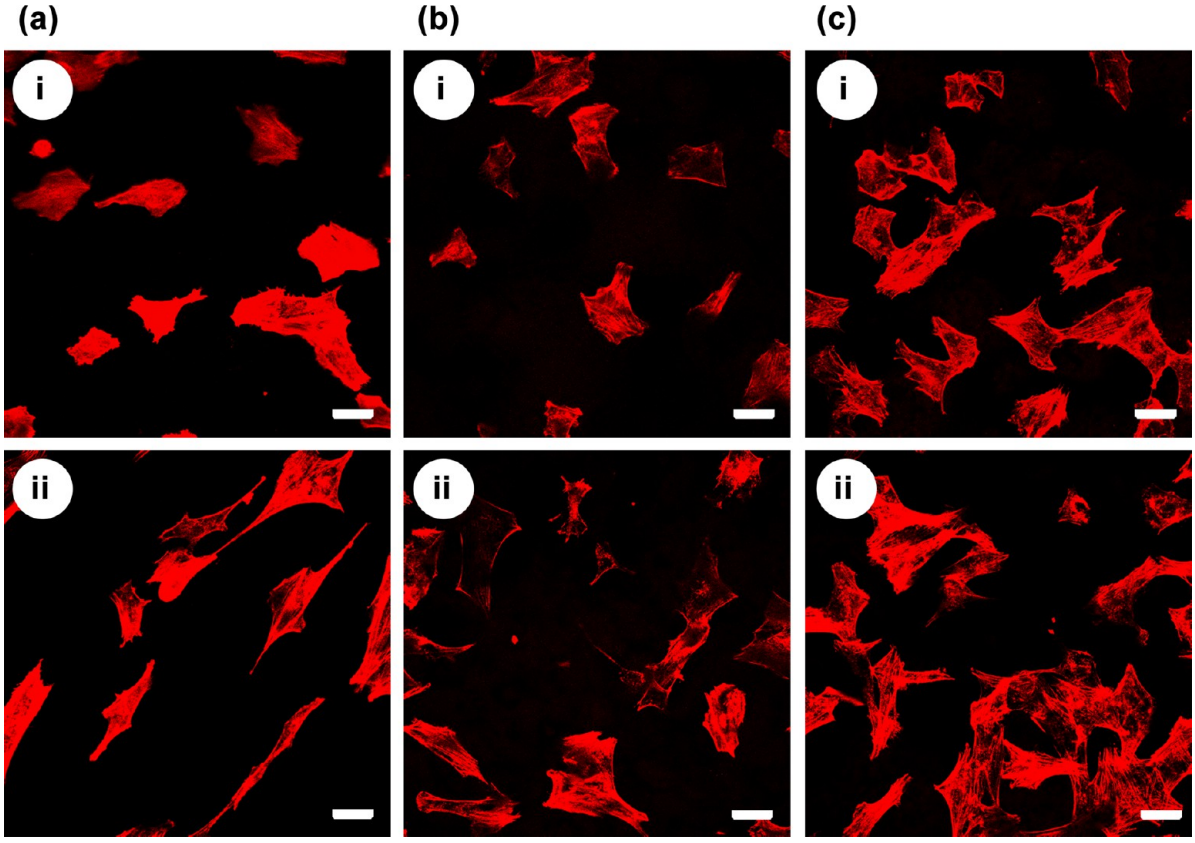

Figure 8. CLSM images of the cytoskeleton of MC3T3-E1 cells grown on UHMWPE (a), PEEK (b), and the n-CS/PEEK composite (c) for 12 h (i) and 24 h (ii). The scale bar is 50 μm.

4. DISCUSSION

PEEK is a polymeric material and is currently used in orthopedic clinics.[14] Although PEEK possesses good biocompatibility and satisfactory mechanical properties, its lack of bioactivity may limit its applications for bone repair. Consequently, there have been efforts to incorporate bioactive materials into PEEK to enhance its bioactivity and bone-implant integration. In this study, a bioactive composite containing n-CS and PEEK was fabricated using compounding and injection-molding. The results revealed that the n-CS particles were well distributed in the PEEK matrix. Previous reports have demonstrated that inorganic particles and organic polymers can interact at their interface.[34−37]

After the incorporation of n-CS into PEEK, the elastic modulus and compressive strength of the n-CS/PEEK composite (n-CS content ranging from 0 to 40 wt %) clearly increased with the n-CS content, whereas the tensile strength of the composite decreased slightly compared with PEEK. The composite containing the high n-CS content of 60 wt % resulted in a dramatic reduction in the mechanical strength. The compressive strength and elastic modulus of the composite containing 40 wt % n-CS were significantly higher than those of the composites containing 20 and 60 wt %, suggesting that a weight ratio of approximately 40 wt % would be optimal. Therefore, the composite with 40 wt % n-CS content was selected for further investigation in this study.

The bioperformance of a material are affected by surface hydrophilicity.[38] In the present study, incorporating n-CS into PEEK markedly decreased the water contact angles of the composites, and the values decreased with increasing n-CS content in the composite. The results suggested that incorporating hydrophilic inorganic materials (n-CS) into hydrophobic polymers (PEEK) is a viable way to improve the hydrophilicity of the n-CS/PEEK composites. A previous study has shown that hydrophilic surfaces are better for cell attachment, spreading, and proliferation than hydrophobic surfaces.[39]

A significant characteristic of bioactive materials is their ability to bond with living bone through the formation of a bone-like apatite layer on their surfaces.[11] Therefore, the bone-bonding ability of a biomaterial is often evaluated by examining the apatite-formation ability on its surface in SBF.[29] In this study, an apatite-layer formed on the surface of the n-CS/PEEK composite after immersion in SBF for 7 days, and the apatite-layer gradually became thicker and more compact with longer immersion time. The P peak in the EDS spectrum was considered to be newly developed because no P element existed on the n-CS/PEEK composite before immersion, and the newly deposited P together with Ca formed the apatite layer. The results indicated that the n-CS/PEEK composite exhibited good in vitro bioactivity compared with PEEK.

Based on previous studies, the mechanism of apatite formation on the n-CS/PEEK composite can be suggested as follows.[11,29,40,41] After contacting SBF, the n-CS/PEEK composite initially release Ca^{2+}, which exchange with H^+ in the SBF and form silanol groups (Si−OH). The Si−OH groups are negatively charged and can attract Ca^{2+} by electrostatic interaction. The accumulation of Ca^{2+} on the material surface attracts PO_4^{3-} from the SBF and deposits it on the composite surface, which triggers the formation of apatite nuclei. The apatite nuclei continue to grow by consuming the Ca and P ions in the surrounding fluid to form a thicker apatite layer.

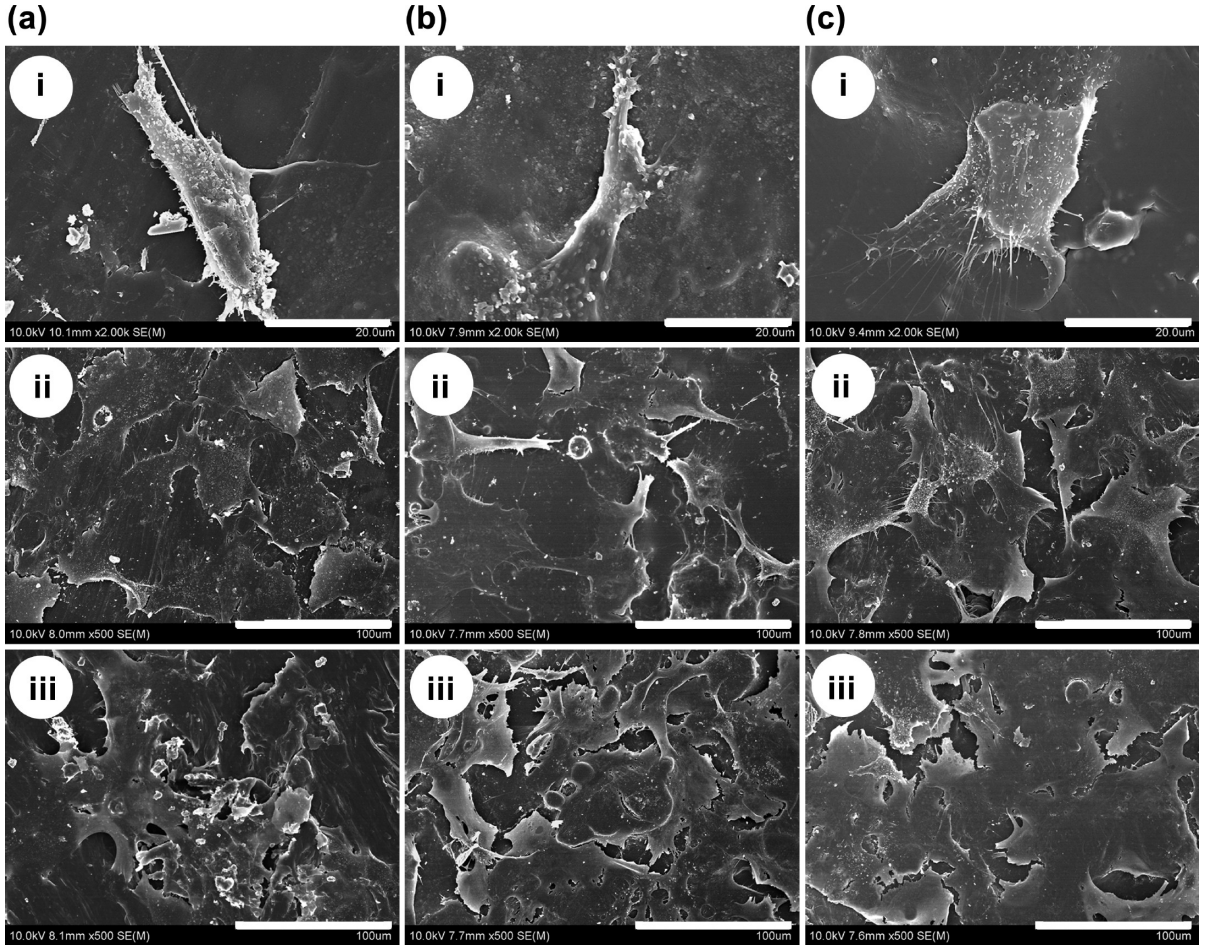

Figure 9. SEM images of the cell morphology and spreading on UHMWPE (a), PEEK (b), and the n-CS/PEEK composite (c) after 1, 3, and 7 days of culture: (i) day 1 (scale bar = 20 μm), (ii) day 3 (scale bar = 100 μm), (iii) day 7 (scale bar = 100 μm).

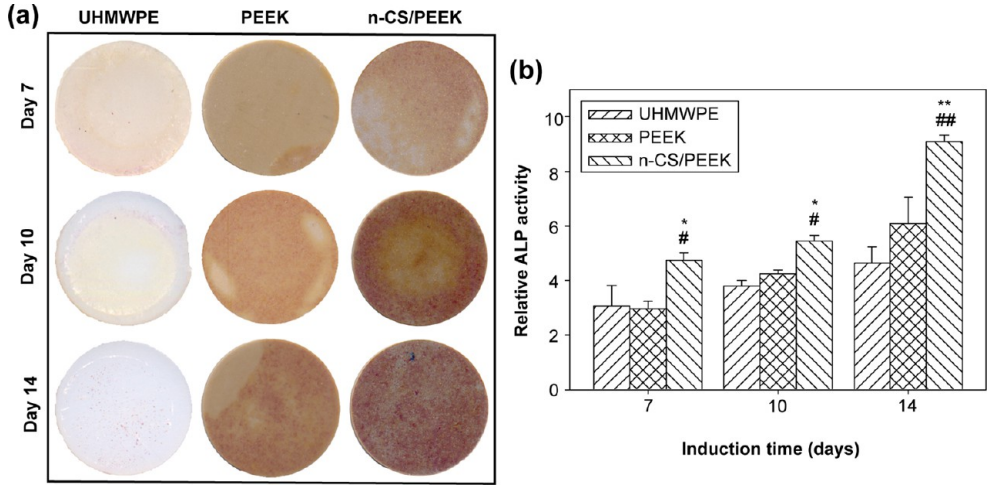

Figure 10. ALP staining and ALP activity of cells grown on UHMWPE, PEEK, and the n-CS/PEEK composite after 7, 10, and 14 days: (a) ALP staining on the material surfaces; (b) quantitative analysis of ALP activity. The ALP activity was normalized to the corresponding content of total protein. "#" and "*" denote significant differences compared with UHMWPE (# $p < 0.05$; ## $p < 0.01$) and PEEK (* $p < 0.05$; ** $p < 0.01$), respectively.

The interaction of cells with a biomaterial surface is a vital element in the evaluation of a biomaterial.[42,43] The initial attachment and spreading of cells will affect the cell proliferation and differentiation on implant materials. Our results indicated that n-CS/PEEK exhibited more attached cells and more efficient cell spreading than PEEK or UHMWPE. These results were attributed to the following three advantages of the n-CS/PEEK composite: the improved hydrophilicity, the generated silanol groups, and the presence of Ca ions. Hydrophilic material surfaces were better for cell attachment, spreading, and cytoskeletal organization than hydrophobic surfaces.[39] In addition, the silanol groups generated by CS can bind to various functional groups of

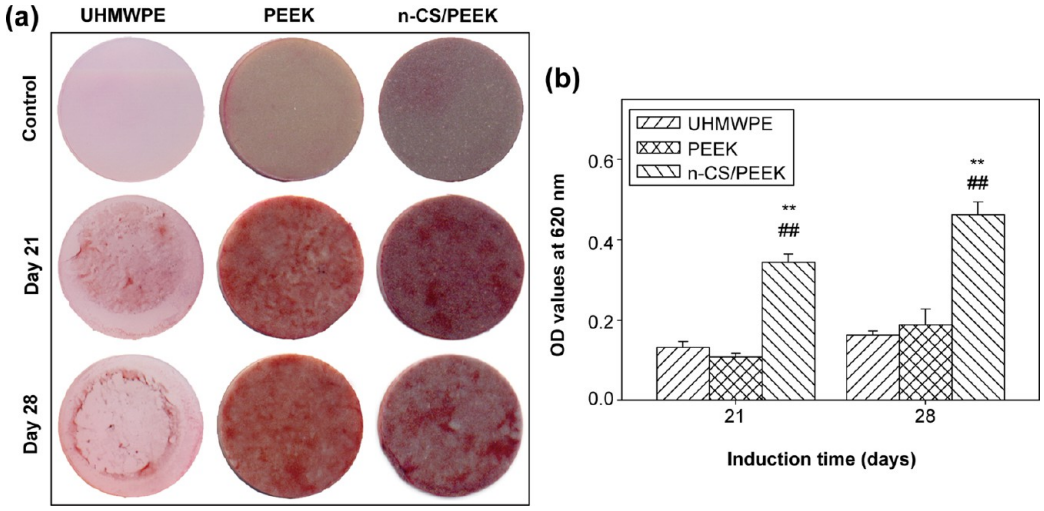

Figure 11. Alizarin red staining and its quantitative analysis on UHMWPE, PEEK, and the n-CS/PEEK composite after 21 and 28 days: (a) alizarin red staining; (b) quantitative analysis of the alizarin red staining. "##" and "**" denote significant differences compared with UHMWPE and PEEK, respectively ($p < 0.01$).

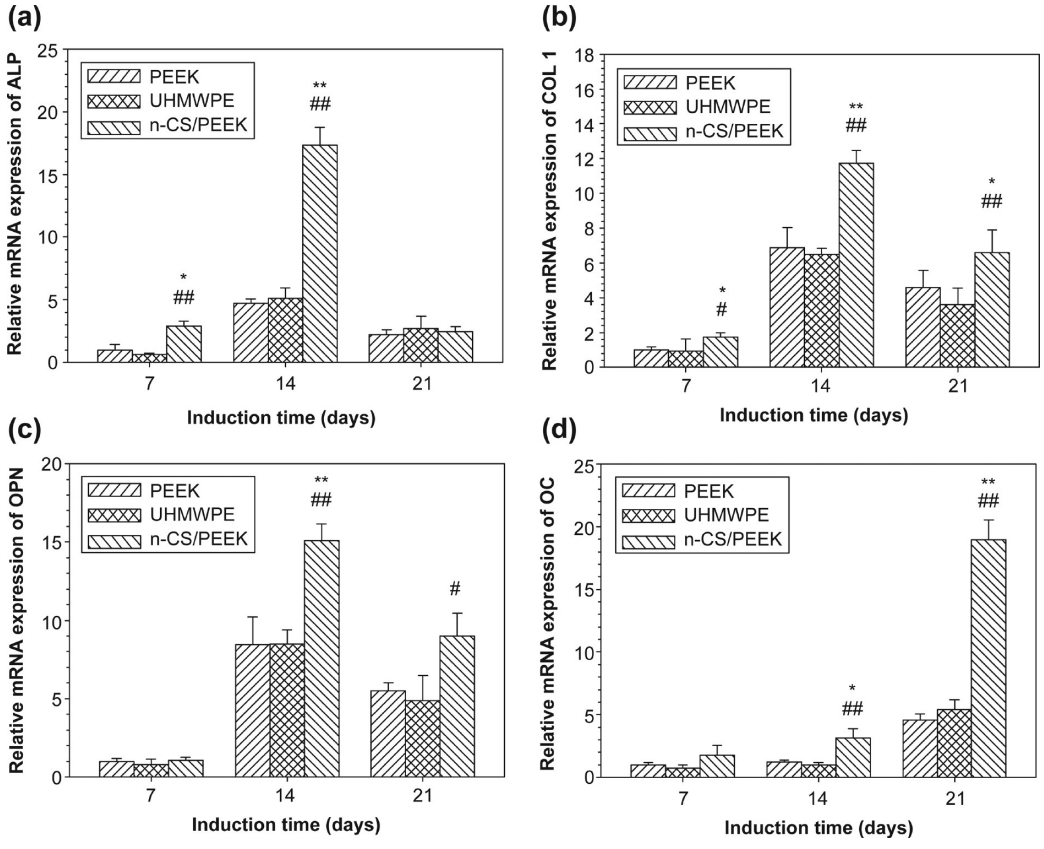

Figure 12. Relative mRNA expression of osteogenic differentiation-related genes in MC3T3-E1 cells grown on UHMWPE, PEEK, and the n-CS/PEEK composite measured by real-time PCR: (a) ALP, (b) COL 1, (c) OPN, (d) OC. The data shown are the mean expression levels relative to β-actin expression and are normalized with respect to the expression levels of cells grown on PEEK at day 7. "#" and "*" denote significant differences compared with UHMWPE (# $p < 0.05$; ## $p < 0.01$) and PEEK (* $p < 0.05$; ** $p < 0.01$), respectively.

proteins via hydrogen bonding or long-range electrostatic ionic amine bonds ($Si{-}O^{-}{-}^{+}H_3N$), thus producing a favorable surface environment for cell attachment.[44] Furthermore, Ca ion sites on the composite surface as ligands of osteoblasts favored protein adsorption due to positive electrostatic attraction.[45] Therefore, the n-CS/PEEK composite with these advantages could exert a positive effect on cell attachment and spreading.

After attachment, cells grown on the material surfaces begin to proliferate. In this study, the n-CS/PEEK composite effectively promoted the proliferation of MC3T3-E1 cells compared with PEEK or UHMWPE. Studies have shown that appropriate Si ions released from silicate-containing materials play an important role in stimulating the proliferation of osteoblasts and bone-marrow stromal cells (BMSCs).[46−48] In addition, the appropriate

Ca ion levels have been shown to stimulate osteoblast proliferation by changing the expression of specific Ca^{2+}-channel isoforms on osteoblasts.[49] Moreover, the formation of an apatite layer on the composite surface has been shown to be beneficial for osteoblast proliferation.[50]

After proliferation, MC3T3-E1 cells begin to produce collagens and other proteins, followed by calcification. ALP activity and calcium deposition are critical factors for osseointegration at the interface between bone tissues and implants.[51,52] In this study, higher ALP activity and more calcium deposition were observed in cells grown on the composite compared with PEEK or UHMWPE. Furthermore, the composite significantly improved the expressions of osteogenic differentiation-related genes, that is, ALP, COL 1, OPN, and OC. The increased ability of osteogenic differentiation on the n-CS/PEEK composite might be mainly related to the Si ions released from the composite. Si ions have been shown to promote mineralized nodule formation, COL 1 synthesis, and the expression of osteogenic-related genes in osteoblasts.[46,47,53] Ca ions released from the composite also played an important role in stimulating osteoblastic differentiation.[49] Furthermore, the apatite formed the composite surface facilitated differentiation of osteoblasts to form an extracellular matrix composed of biological apatite and collagen.[54]

In summary, the n-CS/PEEK composite facilitated the attachment, proliferation, spreading, and differentiation of MC3T3-E1 cells. Therefore, the incorporation of n-CS into PEEK has the potential to greatly improve the bioperformance of PEEK, and the n-CS/PEEK composite exhibited significantly improved biocompatibility and bioactivity compared with PEEK or UHMWPE. Thus, the n-CS/PEEK composite might be a promising bone-repair implant material.

5. CONCLUSIONS

A bioactive composite was fabricated by incorporating n-CS into PEEK using a process of compounding and injection-molding. The results revealed that the mechanical strength of the n-CS/PEEK composites increased with n-CS content up to 40 wt %; however, an n-CS content of 60 wt % led to a substantial decrease of mechanical strength. In addition, the incorporation of n-CS into PEEK greatly improved the hydrophilicity of the composite. Immersion in SBF induced the formation of an apatite layer on the composite, indicating good in vitro bioactivity. In cell tests, the composite significantly promoted the attachment, proliferation, and spreading of MC3T3-E1 cells compared with PEEK or UHMWPE. Furthermore, cells grown on the composite exhibited higher ALP activity, more calcium nodule formation and higher expression levels of osteogenic differentiation-related genes than PEEK or UHMWPE. The positive effects on cellular responses to the composite are most likely due to the improved hydrophilicity of the composite, formed apatite-layer on the composite, and the Si and Ca ions released from the composite. With improved bioactivity and biocompatibility, the n-CS/PEEK biocomposite is believed to be a promising orthopedic implant material for bone repair application.

AUTHOR INFORMATION

Corresponding Authors

*Tel.: +86-21-2327-1133. Fax: +86-21-6313-7020. Email: tingtingtang@hotmail.com.
*Email: jiewei7860@sina.com.

Author Contributions

The manuscript was written with contributions from all the authors. All the authors have approved of the final version of the manuscript.

Notes

The authors declare no competing financial interest.

ACKNOWLEDGMENTS

This research was financially supported by the National Natural Science Foundation of China (Nos. 31271015, 81271705, and 51173041) and the Shanghai Science and Technology Development Fund (Nos. 13DZ2294000, 13JC1403900, 12nm0500400, and 12441903600).

ABBREVIATIONS

n-CS = nanocalcium silicate
PEEK = polyetheretherketone
SBF = simulated body fluid
UHMWPE = ultrahigh molecular weight polyethylene
ALP = alkaline phosphatase
CS = calcium silicate
DMF = dimethylformamide
SEM = scanning electron microscopy
EDS = energy dispersive spectrometry
XRD = X-ray diffraction
FTIR = Fourier transform infrared spectroscopy
Ca = calcium
P = phosphorus
Si = silicon
ICP-AES = inductively coupled plasma atomic emission spectroscopy
DMEM = Dulbecco's Modified Eagle Medium
FBS = fetal bovine serum
CCK-8 = cell counting kit-8
PBS = phosphate-buffered saline
OD = optical density
CLSM = confocal laser scanning microscopy
HMDS = hexamethyldisilazane
COL 1 = collagen type I
OPN = osteoprotein
OC = osteocalcin
PCR = polymerase chain reaction
F = forward
R = reverse
ANOVA = analysis of variance
LSD = least significant difference
Si−OH = silanol groups
BMCs = bone-marrow stromal cells (BMSCs)

REFERENCES

(1) Gopi, D.; Indira, J.; Kavitha, L.; Sekar, M.; Mudali, U. K. Synthesis of hydroxyapatite nanoparticles by a novel ultrasonic assisted with mixed hollow sphere template method. *Spectrochim. Acta, Part A* **2012**, *93*, 131−134.
(2) Gopi, D.; Shinyjoy, E.; Sekar, M.; Surendiran, M.; Kavitha, L.; Sampath Kumar, T. S. Development of carbon nanotubes reinforced hydroxyapatite composite coatings on titanium by electrodeposition method. *Corros. Sci.* **2013**, *73*, 321−330.
(3) Gopi, D.; Nithiya, S.; Shinyjoy, E.; Kavitha, L. Spectroscopic investigation on formation and growth of mineralized nanohydroxyapatite for bone tissue engineering applications. *Spectrochim. Acta, Part A* **2012**, *92*, 194−200.

(4) Salinas, A. J.; Shruti, S.; Malavasi, G.; Menabue, L.; Vallet-Regi, M. Substitutions of cerium, gallium, and zinc in ordered mesoporous bioactive glasses. *Acta Biomater.* **2011**, *7*, 3452−3458.
(5) Looney, M.; O'Shea, H.; Redington, W.; Kelly, G.; Boyd, D. High-temperature X-ray analysis of phase evolution in Sr-doped zinc-silicate glasses. *J. Non-Cryst. Solids* **2011**, *357*, 2097−2102.
(6) Duan, W.; Ning, C.; Tang, T. Cytocompatibility and osteogenic activity of a novel calcium phosphate silicate bioceramic: Silicocarnotite. *J. Biomed Mater. Res. A* **2013**, *101*, 1955−1961.
(7) Schneider, O. D.; Weber, F.; Brunner, T. J.; Loher, S.; Ehrbar, M.; Schmidlin, P. R.; Stark, W. J. In vivo and in vitro evaluation of flexible, cottonwool-like nanocomposites as bone substitute material for complex defects. *Acta Biomater.* **2009**, *5*, 1775−1784.
(8) Dinarvand, P.; Seyedjafari, E.; Shafiee, A.; Jandaghi, A. B.; Doostmohammadi, A.; Fathi, M. H.; Farhadian, S.; Soleimani, M. New approach to bone tissue engineering: Simultaneous application of hydroxyapatite and bioactive glass coated on a poly(L-lactic acid) scaffold. *ACS Appl. Mater. Interfaces* **2011**, *3*, 4518−4524.
(9) Li, X.; Cui, R.; Liu, W.; Sun, L.; Yu, B.; Fan, Y.; Feng, Q.; Cui, F.; Watari, F. The use of nanoscaled fibers or tubes to improve biocompatibility and bioactivity of biomedical materials. *J. Nanomater.* **2013**, *2013*, 1−16.
(10) Xie, X.; Yu, X.; Zeng, S.; Du, R.; Hu, Y.; Yuan, Z.; Lu, E.; Dai, K.; Tang, T. Enhanced osteointegration of orthopaedic implant gradient coating composed of bioactive glass and nanohydroxyapatite. *J. Mater. Sci. Mater. Med.* **2010**, *21*, 2165−2173.
(11) Kokubo, T.; Kim, H.-M.; Kawashita, M. Novel bioactive materials with different mechanical properties. *Biomaterials* **2003**, *24*, 2161−2175.
(12) Ma, R.; Tang, T. Current strategies to improve the bioactivity of PEEK. *Int. J. Mol. Sci.* **2014**, *15*, 5426−5445.
(13) Luo, H.; Xiong, G.; Yang, Z.; Raman, S. R.; Li, Q.; Ma, C.; Li, D.; Wang, Z.; Wan, Y. Preparation of three-dimensional braided carbon fiber-reinforced PEEK composites for potential load-bearing bone fixations. Part I. Mechanical properties and cytocompatibility. *J. Mech. Behav. Biomed. Mater.* **2014**, *29*, 103−113.
(14) Kurtz, S. M.; Devine, J. N. PEEK biomaterials in trauma, orthopedic, and spinal implants. *Biomaterials* **2007**, *28*, 4845−4869.
(15) Zhao, Y.; Wong, H. M.; Wang, W.; Li, P.; Xu, Z.; Chong, E. Y.; Yan, C. H.; Yeung, K. W.; Chu, P. K. Cytocompatibility, osseointegration, and bioactivity of three-dimensional porous and nanostructured network on polyetheretherketone. *Biomaterials* **2013**, *34*, 9264−9277.
(16) Anderson, J. M. Biological responses to materials. *Annu. Rev. Mater. Res.* **2001**, *31*, 81−110.
(17) Meyers, S. R.; Khoo, X.; Huang, X.; Walsh, E. B.; Grinstaff, M. W.; Kenan, D. J. The development of peptide-based interfacial biomaterials for generating biological functionality on the surface of bioinert materials. *Biomaterials* **2009**, *30*, 277−286.
(18) Mehrali, M.; Moghaddam, E.; Shirazi, S. F.; Baradaran, S.; Mehrali, M.; Latibari, S. T.; Metselaar, H. S.; Kadri, N. A.; Zandi, K.; Osman, N. A. Synthesis, mechanical properties, and in vitro biocompatibility with osteoblasts of calcium silicate-reduced graphene oxide composites. *ACS Appl. Mater. Interfaces* **2014**, *6*, 3947−3962.
(19) Wu, C.; Chang, J. A review of bioactive silicate ceramics. *Biomed. Mater.* **2013**, *8*, 032001.
(20) Li, H.; Chang, J. Stimulation of proangiogenesis by calcium silicate bioactive ceramic. *Acta Biomater* **2013**, *9*, 5379−5389.
(21) Liu, X.; Morra, M.; Carpi, A.; Li, B. Bioactive calcium silicate ceramics and coatings. *Biomed. Pharmacother.* **2008**, *62*, 526−529.
(22) Ding, S. J.; Shie, M. Y.; Wei, C. K. In vitro physicochemical properties, osteogenic activity, and immunocompatibility of calcium silicate-gelatin bone grafts for load-bearing applications. *ACS Appl. Mater. Interfaces* **2011**, *3*, 4142−4153.
(23) Wang, C.; Lin, K.; Chang, J.; Sun, J. The stimulation of osteogenic differentiation of mesenchymal stem cells and vascular endothelial growth factor secretion of endothelial cells by β-$CaSiO_3$/β-Ca_3 $(PO4)_2$ scaffolds. *J. Biomed Mater. Res. A* **2014**, *102*, 2096−2104.
(24) Fei, L.; Wang, C.; Xue, Y.; Lin, K.; Chang, J.; Sun, J. Osteogenic differentiation of osteoblasts induced by calcium silicate and calcium silicate/β-tricalcium phosphate composite bioceramics. *J. Biomed. Mater. Res. B Appl. Biomater.* **2012**, *100*, 1237−1244.
(25) Li, M.; Liu, W.; Sun, J.; Xianyu, Y.; Wang, J.; Zhang, W.; Zheng, W.; Huang, D.; Di, S.; Long, Y. Z.; Jiang, X. Culturing primary human osteoblasts on electrospun poly(lactic-co-glycolic acid) and poly(lactic-co-glycolic acid)/nanohydroxyapatite scaffolds for bone tissue engineering. *ACS Appl. Mater. Interfaces* **2013**, *5*, 5921−5926.
(26) Lu, L. X.; Zhang, X. F.; Wang, Y. Y.; Ortiz, L.; Mao, X.; Jiang, Z. L.; Xiao, Z. D.; Huang, N. P. Effects of hydroxyapatite-containing composite nanofibers on osteogenesis of mesenchymal stem cells in vitro and bone regeneration in vivo. *ACS Appl. Mater. Interfaces* **2013**, *5*, 319−330.
(27) Heinemann, S.; Heinemann, C.; Jager, M.; Neunzehn, J.; Wiesmann, H. P.; Hanke, T. Effect of silica and hydroxyapatite mineralization on the mechanical properties and the biocompatibility of nanocomposite collagen scaffolds. *ACS Appl. Mater. Interfaces* **2011**, *3*, 4323−4331.
(28) Li, D.; Sun, H.; Jiang, L.; Zhang, K.; Liu, W.; Zhu, Y.; Fangteng, J.; Shi, C.; Zhao, L.; Sun, H.; Yang, B. Enhanced biocompatibility of PLGA nanofibers with gelatin/nano-hydroxyapatite bone biomimetics incorporation. *ACS Appl. Mater. Interfaces* **2014**, *6*, 9402−9410.
(29) Kokubo, T.; Takadama, H. How useful is SBF in predicting in vivo bone bioactivity? *Biomaterials* **2006**, *27*, 2907−2915.
(30) Fan, Q.; Tang, T.; Zhang, X.; Dai, K. The role of CCAAT/enhancer binding protein (C/EBP)-α in osteogenesis of C3H10T1/2 cells induced by BMP-2. *J. Cell Mol. Med.* **2009**, *13*, 2489−2505.
(31) Wan, X.; Chang, C.; Mao, D.; Jiang, L.; Li, M. Preparation and in vitro bioactivities of calcium silicate nanophase materials. *Mater. Sci. Eng., C* **2005**, *25*, 455−461.
(32) Yu, S.; Hariram, K. P.; Kumar, R.; Cheang, P.; Aik, K. K. In vitro apatite formation and its growth kinetics on hydroxyapatite/polyetheretherketone biocomposites. *Biomaterials* **2005**, *26*, 2343−2352.
(33) Ni, S.; Chang, J.; Chou, L. A novel bioactive porous $CaSiO_3$ scaffold for bone tissue engineering. *J. Biomed Mater. Res. A* **2006**, *76*, 196−205.
(34) Cho, S. B.; An, E. M.; Lee, S.; Jang, H. D.; Kim, I. Y.; Ohtsuki, C.; Kim, Y. J. Effects of heat treatment on apatite formation of CaO-SiO_2-PEEK composites. *Key Eng. Mater.* **2012**, *529*−*530*, 436−440.
(35) Parvinzadeh, M.; Moradian, S.; Rashidi, A.; Yazdanshenas, M.-E. Surface characterization of polyethylene terephthalate/silica nanocomposites. *Appl. Surf. Sci.* **2010**, *256*, 2792−2802.
(36) Gashti, M. P.; Stir, M.; Hulliger, J. Synthesis of bone-like microporous calcium phosphate/iota-carrageenan composites by gel diffusion. *Colloids Surf., B* **2013**, *110*, 426−433.
(37) Pan, Y. S.; Wang, J.; Pan, C. L. Research on biological properties of PEEK based composites. *Appl. Mech. Mater.* **2013**, *325*−*326*, 3−7.
(38) Shen, Y.; Ma, Y.; Gao, M.; Lai, Y.; Wang, G.; Yu, Q.; Cui, F. Z.; Liu, X. Integrins-FAK-Rho GTPases pathway in endothelial cells sense and response to surface wettability of plasma nanocoatings. *ACS Appl. Mater. Interfaces* **2013**, *5*, 5112−5121.
(39) Altankov, G.; Grinnell, F.; Groth, T. Studies on the biocompatibility of materials: Fibroblast reorganization of substratum-bound fibronectin on surfaces varying in wettability. *J. Biomed Mater. Res.* **1996**, *30*, 385−391.
(40) Liu, X.; Ding, C.; Chu, P. K. Mechanism of apatite formation on wollastonite coatings in simulated body fluids. *Biomaterials* **2004**, *25*, 1755−1761.
(41) Kaur, G.; Pandey, O. P.; Singh, K.; Homa, D.; Scott, B.; Pickrell, G. A review of bioactive glasses: Their structure, properties, fabrication, and apatite formation. *J. Biomed Mater. Res. A* **2014**, *102*, 254−275.
(42) Moura, C. G.; Souza, M. A.; Kohal, R. J.; Dechichi, P.; Zanetta-Barbosa, D.; Jimbo, R.; Teixeira, C. C.; Teixeira, H. S.; Tovar, N.; Coelho, P. G. Evaluation of osteogenic cell culture and osteogenic/peripheral blood mononuclear human cell co-culture on modified titanium surfaces. *Biomed. Mater.* **2013**, *8*, 035002.
(43) Tan, H.; Guo, S.; Yang, S.; Xu, X.; Tang, T. Physical characterization and osteogenic activity of the quaternized chitosan-loaded PMMA bone cement. *Acta Biomater.* **2012**, *8*, 2166−2174.

(44) Lobel, K. D.; Hench, L. L. In vitro adsorption and activity of enzymes on reaction layers of bioactive glass substrates. *J. Biomed Mater. Res.* **1998**, *39*, 575−579.
(45) Feng, B.; Weng, J.; Yang, B. C.; Qu, S. X.; Zhang, X. D. Characterization of titanium surfaces with calcium and phosphate and osteoblast adhesion. *Biomaterials* **2004**, *25*, 3421−3428.
(46) Zhai, W.; Lu, H.; Wu, C.; Chen, L.; Lin, X.; Naoki, K.; Chen, G.; Chang, J. Stimulatory effects of the ionic products from Ca-Mg-Si bioceramics on both osteogenesis and angiogenesis in vitro. *Acta Biomater.* **2013**, *9*, 8004−8014.
(47) Han, P.; Wu, C.; Xiao, Y. The effect of silicate ions on proliferation, osteogenic, differentiation, and cell signalling pathways (WNT and SHH) of bone marrow stromal cells. *Biomater Sci.* **2013**, *1*, 379−392.
(48) Hoppe, A.; Guldal, N. S.; Boccaccini, A. R. A review of the biological response to ionic dissolution products from bioactive glasses and glass-ceramics. *Biomaterials* **2011**, *32*, 2757−2774.
(49) Maeno, S.; Niki, Y.; Matsumoto, H.; Morioka, H.; Yatabe, T.; Funayama, A.; Toyama, Y.; Taguchi, T.; Tanaka, J. The effect of calcium ion concentration on osteoblast viability, proliferation, and differentiation in monolayer and 3D culture. *Biomaterials* **2005**, *26*, 4847−4855.
(50) Sarmento, C.; Luklinska, Z. B.; Brown, L.; Anseau, M.; De Aza, P. N.; De Aza, S.; Hughes, F. J.; McKay, I. J. In vitro behavior of osteoblastic cells cultured in the presence of pseudowollastonite ceramic. *J. Biomed Mater. Res. A* **2004**, *69*, 351−358.
(51) Lin, W. T.; Tan, H. L.; Duan, Z. L.; Yue, B.; Ma, R.; He, G.; Tang, T. T. Inhibited bacterial biofilm formation and improved osteogenic activity on gentamicin-loaded titania nanotubes with various diameters. *Int. J. Nanomed.* **2014**, *9*, 1215−1230.
(52) Ao, H.; Xie, Y.; Tan, H.; Yang, S.; Li, K.; Wu, X.; Zheng, X.; Tang, T. Fabrication and in vitro evaluation of stable collagen/hyaluronic acid biomimetic multilayer on titanium coatings. *J. R Soc. Interface* **2013**, *10*, 20130070.
(53) Sun, J.; Wei, L.; Liu, X.; Li, J.; Li, B.; Wang, G.; Meng, F. Influences of ionic dissolution products of dicalcium silicate coating on osteoblastic proliferation, differentiation and gene expression. *Acta Biomater.* **2009**, *5*, 1284−1293.
(54) Loty, C.; Sautier, J. M.; Boulekbache, H.; Kokubo, T.; Kim, H. M.; Forest, N. In vitro bone formation on a bone-like apatite layer prepared by a biomimetic process on a bioactive glass−ceramic. *J. Biomed. Mater. Res.* **2000**, *49*, 423−434.